

Which E_{peak} ? – The Characteristic Energy of Gamma-Ray Burst Spectra

Robert Preece

Space Science Department, The University of Alabama in Huntsville, Huntsville, AL 35809

Adam Goldstein

Space Science Office, VP62, NASA/Marshall Space Flight Center, Huntsville, AL 35812

Narayana Bhat and Matthew Stanbro

Center for Space Plasma and Aeronomic Research, The University of Alabama in Huntsville, Huntsville, AL 35809

Jon Hakkila

The University of Charleston, SC at the College of Charleston 29424
and

Dylan Blalock

Physics Department, The University of Alabama in Huntsville, Huntsville, AL 35809

ABSTRACT

A characteristic energy of individual gamma-ray burst (GRB) spectra can in most cases be determined from the peak energy of the energy density spectra ($\nu\mathcal{F}_\nu$), called ‘ E_{peak} ’. Distributions of E_{peak} have been compiled for time-resolved spectra from bright GRBs, and also time-averaged spectra and peak flux spectra for nearly every burst observed by CGRO-BATSE and Fermi-GBM. Even when determined by an instrument with a broad energy band, such as GBM (8 keV to 40 MeV), the distributions themselves peak at around 240 keV in the observer’s frame, with a spread of roughly a decade in energy. E_{peak} can have considerable evolution (sometimes greater than one decade) within any given burst, as amply demonstrated by single pulses in GRB110721A and GRB130427A. Meanwhile, several luminosity or energy relations have been proposed to correlate with either the time-integrated or peak flux E_{peak} . Thus, when discussing correlations with E_{peak} , the question arises, “Which E_{peak} ?”. A single burst may be characterized by any one of a number of values for E_{peak} that are associated with it. Using a single pulse simulation model with spectral evolution as a proxy for the type of spectral evolution observed in many bursts, we investigate how the time-averaged E_{peak} emerges from the spectral evolution within a single pulse, how this average naturally correlates with the peak flux derived E_{peak} in a burst and how the distribution in E_{peak} values from many bursts derives its surprisingly narrow width.

Subject headings: (stars:) gamma-ray burst: general — methods: data analysis

1. Introduction

Unquestionably, a characteristic energy can be an important diagnostic feature of the spectra of cosmological sources. If the sources are standard in some way, with identifiable atomic or nuclear lines, for example, the energy measurement could then directly correspond with distance via the cosmological redshift. From early on, analyses of the prompt emission of gamma-ray bursts (GRBs) revealed that a spectral break typically occurred within the instrumental pass band of scintillator-based detectors – between approximately 20 keV to 1 MeV (Mazets & Golenetskii 1995; Metzger et al. 1974; Harris & Share 1998). The spectral break can take on the form of an exponentially-attenuated power-law; in which case, it had been associated with an optically-thin thermal bremsstrahlung temperature. However, many burst spectra are typically harder than thermal, with a high-energy tail that may be characterized by a power law. This led Band et al. (1993) to propose an entirely phenomenological spectral form that is the unique function joining two power laws that is continuous and smooth to first order: the ‘Band’ GRB function. This function finds its most familiar form in equation 1, in a parametrization where the break energy is cast as the peak in the spectral energy distribution ($E^2 f_{\text{Band}}(E)$ or $\nu \mathcal{F}_\nu$): E_{peak} .

$$\begin{aligned}
 f_{\text{Band}}(E) &= A \left(\frac{E}{100 \text{ keV}} \right)^\alpha \exp \left(-\frac{E(2+\alpha)}{E_{\text{peak}}} \right) \\
 \text{if } E < \frac{(\alpha-\beta) E_{\text{peak}}}{(2+\alpha)} &\equiv E_{\text{break}}, \\
 f_{\text{Band}}(E) &= A \left[\frac{(\alpha-\beta) E_{\text{peak}}}{(2+\alpha) 100 \text{ keV}} \right]^{(\alpha-\beta)} \times \\
 &\quad \exp(\beta-\alpha) \left(\frac{E}{100 \text{ keV}} \right)^\beta \\
 \text{if } E \geq \frac{(\alpha-\beta) E_{\text{peak}}}{(2+\alpha)}. & \quad (1)
 \end{aligned}$$

From the form of the function, both α and β are power law indices in photon number. Because of the pre-factor E^2 in the definition of $\nu \mathcal{F}_\nu$, E_{peak} is only defined for values of β less than -2 (as is typical). For large negative values of β , we recover thermal-like spectra, guaranteed to yield a value for E_{peak} as long as $\alpha > -2$. With three shape parameters, the Band function is flexible

enough to stand in for a number of physical processes likely to occur in GRBs, including blackbody emission, synchrotron emission by thermal or power law electrons, as well as Compton scattering in any of its various guises. However, the Band function has a specific constant curvature that does not match any of these in detail, especially in the region where the two power law segments join (e.g.: see figure 8 in Burgess et al. (2014)).

For the purposes of the current work, it is more convenient to use a cut-off model power-law (the so-called COMP function in the spectral fitting package RMFIT¹), which is identical to the Band function in the limit $\beta \rightarrow -\infty$. The COMP functional form can also be cast in terms of E_{peak} , as shown in equation 2.

$$f_{\text{COMP}}(E) = A \left(\frac{E}{100 \text{ keV}} \right)^\alpha \exp \left(-\frac{E(2+\alpha)}{E_{\text{peak}}} \right). \quad (2)$$

There are several reasons that drive our choice of this function for the simulations described below. First, for most bursts where the spectral evolution can be determined as a function of time, it is possible to create time slices that can track the evolution of E_{peak} (and α) with good precision, while for the same temporal accumulations, β can not be determined with any precision. The reason for this is that both the effective area and the flux fall rapidly with increasing energy, resulting in too few counts above E_{peak} to determine the spectrum. Indeed, one of the results from the Compton Observatory’s Burst And Transient Source Experiment (BATSE) Catalog of time-resolved spectroscopy of bright bursts (Kaneko et al. 2006) was that the COMP function was preferred over the Band function in a majority of the spectra fit (34.9% vs. 33.7% for the BEST model; see Table 8 in the Catalog). It is possible that some GRB spectra arise from synchrotron emission from thermal electrons, especially just after the photosphere has become optically thin. In that case, the emission should resemble the COMP function with $\alpha \sim -2/3$. Even when a Band function fit is preferred, for example, as in the spectral analysis of the first pulse of the bright GRB 130427A (Preece et al. 2014), the

¹RMFIT version 4.4.2 was used throughout this work. RMFIT is publicly available at NASA’s HEASARC website: <http://Fermi.gsfc.nasa.gov/ssc/data/analysis/rmfrit>.

Band β parameter was required to be held fixed for each 0.1 s accumulation; otherwise, the extra free parameter creates instabilities in the fits to the other parameters, due to their high degree of cross-correlation (as noted in, e.g., Kaneko et al. (2006)). Finally, the sum of several exponentials evolving under certain conditions can approximate a power law, as we shall show below. Conversely, the sum of many power laws with different spectral indices is guaranteed not to result in a power law. It is one of the outstanding questions of GRB spectroscopy why the data should ever be consistent with the Band function.

As mentioned above, assuming it represents a characteristic energy, E_{peak} is the unique spectral parameter that encodes relative motion between the source and the observer. Given that GRB redshifts have been measured for many events, the distribution of these currently falls between $z \approx 0.01$ (Galama et al. 1998) and $z \approx 9.4$ (Cucchiara et al. 2011), with a peak between $z = 1$ and 2. Without any other consideration, we might expect the distribution of E_{peak} to follow the redshift distribution, with the smallest values corresponding with the largest redshifts. However, there is good reason to suspect that the GRB emission arises within a relativistic blast wave (Rees & Mészáros 1994). Any characteristic energy, as seen in the observer’s frame, should thus also be multiplied by the bulk Lorentz factor Γ :

$$E_{\text{obs}} = E_{\text{src}}\Gamma/(z + 1), \quad (3)$$

where the characteristic energy at the source is E_{src} . Under the most common assumptions, a limit on the bulk Lorentz factor can be determined as follows: the blast wave must be optically thin to its own photons, otherwise it would still be a fireball, due to photon-photon pair production. The emission from a relativistic blast wave is highly beamed, raising the pair-production energy threshold to $1 \text{ MeV } \Gamma/\gamma > 1$, for photons with energies of γ , in units of the electron’s rest energy. A more careful treatment would have to include details of the spectrum against which the highest energy photon is scattering (Baring & Harding 1997; Baring 2006). Thus, in the simplest case, if a photon with energy γ is observed, it puts a limit on the bulk Lorentz factor $\Gamma > \gamma$. Thus, Γ , as determined by the maximum observed photon energy, is found to vary from burst to burst. The intrinsic

variability of the central engine or the possibility that relativistic shock collisions accelerate particles at the expense of Γ (Rees & Mészáros 1994), make it very likely that Γ is expected to vary *during* a burst. All of these factors are reflected in the observed values and evolution of E_{peak} .

However, it is clearly true that E_{peak} arises from some *physical* emission process, so on top of the known sources of potential variation on the observed quantity, there is an unknown intrinsic distribution in E_{peak} that is related to the underlying physical processes. This intrinsic distribution may be quite wide, as can be seen in the time-resolved spectra of single-pulse bursts where the redshift is known, like GRB110721A (Axelsson et al. 2012) and the first pulse of GRB130427A (Preece et al. 2014). In each of these, hard-to-soft spectral evolution was observed, with E_{peak} varying over considerably greater than one decade in energy. Despite the supposition that each of the contributions to the variation in E_{peak} should operate completely independently, the overall distribution of fitted values of E_{peak} is less than a decade in width (e.g.: Figure 1, discussed below), whether the distribution is drawn from the average spectra of a large sample of bursts (Goldstein et al. 2013; Nava et al. 2012; Gruber et al. 2014) or from statistically independent time-resolved spectra from bright bursts (Kaneko et al. 2006). Much has been made of broad correlations between E_{peak} and other measured quantities, such as the total (isotropic) energy, as in the relation of Amati et al. (2002). Such relations could be useful for obtaining red-shifts directly from spectral measurements, for example. However, several groups have analyzed such relations and claim that they are artifacts of selection effects (Nakar & Piran 2005; Band & Preece 2005; Schaefer & Collazzi 2007).

For those spectra where E_{peak} values could be determined reliably, the distribution roughly resembles a log-normal function of approximately a decade in width (e.g.: the ‘GOOD’ set as seen in Figure 11 from Kaneko et al. (2006)). The specific shape of the distribution is not specified by any theory; so the paucity of low- and high-energy E_{peak} values has widely been attributed to detector selection effects. Still, it is not known why E_{peak} should not be evenly distributed between the lowest and highest energy bounds of the detector. It was speculated that once the

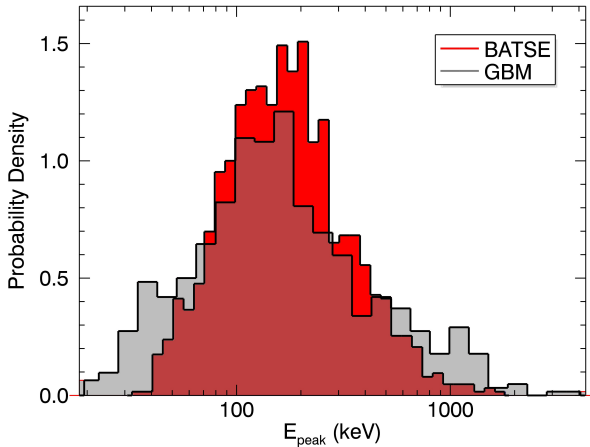


Fig. 1.— Histograms of the E_{peak} values derived from fluence-averaged spectra, comprised of 1297 BATSE bursts (grey - Goldstein et al. (2013)) and 680 GBM bursts (red - Gruber et al. (2014)). The extended spectral coverage of GBM clearly shows up in the enhancement of bursts found in the low- and high-energy wings. The widths of the two distributions are qualitatively similar.

Fermi Gamma-ray Burst Monitor (GBM) flew, the question of the reality of the high-energy cutoff of this distribution would be settled (Piran, Sari & Mochkovitch 2012). It has; the E_{peak} distribution cutoff for GBM, relative to BATSE, does not change all that much, even though GBM has the medium-energy (200 keV to 40 MeV) range of the BGO detectors to contribute to the spectral fitting. Figure 1 shows a comparison between the fluence (average spectrum) E_{peak} values between the BATSE and GBM data sets (Goldstein et al. 2013; Gruber et al. 2014), indicating that GBM extends the distribution by including more lower and higher energy values. That is not to say that there are *no* spectra with large values of E_{peak} , just that the majority of fitted E_{peak} values cluster around a 200 keV value. Certainly, there is no ‘undiscovered country’ of E_{peak} values clustering in the MeV range. We will explore why this might be in this paper.

In order to facilitate understanding of the important role E_{peak} plays in the various observed correlations with other burst observables, we ex-

amine herein various factors that can affect the observed values of E_{peak} . First of all, in section 2, we examine the limits of detectability of a single value for E_{peak} from simulations of spectra of increasingly diminished intensity. Next, in section 3, we look at simulations of hard-to-soft pulses and the role of spectral evolution in the determination of average values of E_{peak} . In section 4, we look at simulations of multiple, overlapping hard-to-soft pulses. Finally, we examine some intrinsic correlations that arise naturally in pulses with spectral evolution.

2. Limits on E_{peak} Detectability

By simulating ~ 15000 different spectra via varying all Band function parameters on a spectral grid using GBM responses, we can study the efficiency of recovering E_{peak} . Figure 2 shows the fraction of Band function fits that include the simulated true value of E_{peak} within the 1σ uncertainty, marginalizing over all inputs of the amplitude, alpha, and beta. We find that E_{peak} can be reliably recovered between ~ 20 keV–40 MeV. Considering that the GBM bandpass is 8 keV–40 MeV, nearly all E_{peak} values that exist within the GBM band can be reliably recovered via spectral fitting. The low point at 600 keV represents a roughly $1 - 2\sigma$ fluctuation. Because the estimation and constraint of the Band function curvature is dependent on the low-energy index, E_{peak} values < 20 keV observed by GBM are unlikely to be constrained because there is insufficient data to constrain the low-energy index. In this case, the spectrum would appear similar to a simple power law with an index similar to the index of the Band high-energy index. Figure 27b in Goldstein et al. (2013) presents a similar set of simulations with BATSE with similar findings. Due to the narrower energy band of BATSE (20–2000 keV) with respect to GBM, there was also an apparent decrease in accuracy if E_{peak} existed above the detector band, although the loss of accuracy was not as dramatic compared to the low- E_{peak} case. The interpretation for the high- E_{peak} case is that as long as the low-energy index is reasonably constrained and some curvature is measurable within the detector band, then it is possible to estimate E_{peak} , albeit with less accuracy and constraint. It is in part to avoid the issue of the interplay between fitting E_{peak} and β in the Band function

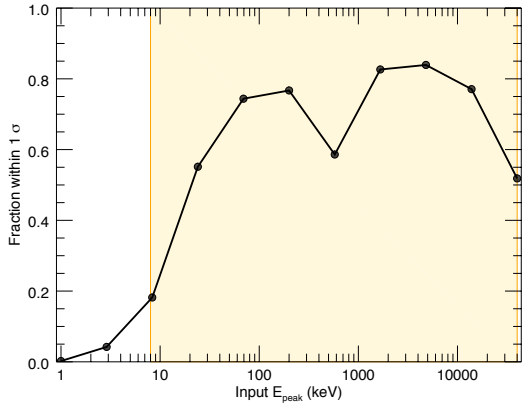


Fig. 2.— Plot of the fraction of Band function fits that contain the simulated input E_{peak} energy within the 1σ confidence interval of the fits. The simulations were performed over a grid of amplitude, alpha, beta, and E_{peak} values and the plot marginalizes over all parameters except E_{peak} . The orange region denotes the GBM energy range.

that we choose to perform our pulse spectral evolution simulations with the COMP function, as discussed above.

3. Hard-to-soft E_{peak} Evolution in Pulses

Recent work has firmly established that pulses, defined as an emission episode with a rise in brightness to a peak followed by a decay, are the prime building blocks that make up the prompt emission light curve in GRBs (Hakkila & Cumbee 2009). One piece of evidence supporting this conclusion is the observation of temporal evolution of E_{peak} throughout many bright, isolated pulses. In the hard-to-soft (HTS) case, E_{peak} evolves smoothly (in many cases as a power law) from an initial high value at the onset of the pulse, through the rising portion, the peak and the decaying portion to a final low energy when the pulse can no longer be detected (Lu et al. 2010; Norris et al. 1996; Axelsson et al. 2012; Preece et al. 2014; Burgess et al. 2014). Another behavior, called hardness-intensity ‘tracking’ (HIT), is where the fitted value of E_{peak} follows the pulse intensity (expressed as integrated counts over a standard

energy range) with good correlation. Hakkila & Preece (2011) and Lu et al. (2010) have both suggested that the tracking behavior may arise when several pulses are run together, so that they may not be clearly distinguished. We will also address this below. In many cases, the rising portion may be too short, compared with the decay, to be able to determine any trend in E_{peak} ; this is common with weaker events, especially if there is only a single spectrum in the rising portion before the peak that is significant enough to obtain a fit. We take this as a motivation for our hypothesis: that signal-to-noise sampling under-emphasizes the lowest and highest energies, which are found preferentially on the rise and decay portions of pulses (true for both HTS and HIT pulses), resulting in the observed narrow distributions.

In this section, we will concentrate on bright, single pulses with HTS behavior. There is ample motivation for this: several very bright bursts are either composed of single pulses or have at least one well-separated pulse with clear HTS evolution. In several of these cases, the temporal evolution of E_{peak} is that of a -1 power law throughout. Since the picture becomes more complicated when physical processes are used to model the emission (in the case of Burgess et al. (2014); Preece et al. (2014), the sum of blackbody and synchrotron was used and the resulting temporal evolution of the characteristic energy was more consistent with a broken power law), we will restrict ourselves here to the evolution of the COMP function parameters.

3.1. A Model Pulse with Spectral Evolution

We start out with a simple simulation of a single pulse with HTS spectral evolution. Following Norris et al. (2005) and Hakkila & Preece (2011), we adopt a parameterized pulse profile:

$$p(t) = \exp(-\tau_1/(t - t_{\text{start}}) - (t - t_{\text{start}})/\tau_2), \quad (4)$$

where τ_1 and τ_2 are the rise and decay times of the pulse and the onset of the pulse is at time t_{start} . In terms of these parameters, the duration of the pulse is approximately

$$t_{\text{dur}} = \tau_2 \sqrt{9 + 12\sqrt{\tau_1/\tau_2}}. \quad (5)$$

Next, we can specify a power-law temporal evolution for E_{peak} from E_{hi} to E_{lo} over the pulse duration t_{dur} by the power-law index:

$$i = \ln(E_{\text{hi}}/E_{\text{lo}})/\ln(t_{\text{dur}} + 1). \quad (6)$$

Finally, the power-law behavior of E_{peak} is expressed as:

$$E_{\text{peak}}(t) = E_{\text{hi}}(t - t_{\text{start}} + 1)^{-i}. \quad (7)$$

All of these quantities are so far continuous; we must discretize the time t into finite width time bins. To simulate a pulse, we then evaluate a photon function for the changing value of E_{peak} in each of the time bins. In the following, we use the exponentially-attenuated cut-off power law form of Eq. 2. This simplifies the analysis for the reasons discussed above: excluding the possible evolution of β , which could lead to complications in the analysis. The photon function is converted to counts data by multiplication by a detector response matrix (DRM). For this to work, the energy bins of the photon function must match those of the specific DRM chosen. Different instruments will have different numbers of ‘input’ photon energy bins, as well as ‘output’ energy-loss bins on the counts side that match a specific instrument’s data types. For this study, we use GBM DRMs from a triggered burst that have 128 output energy bins, corresponding to the CSPEC or TTE data types (Meegan et al. 2009). The result is a realization of a single pulse that consists of a 2D set of numbers that represents count rates in time and energy.

To simulate the correct counts statistics of an observed burst, we first scale the rates to produce some desired peak intensity. This peak count rate is multiplied into the entire 2D pulse model. We then add the background rate (as described below) to obtain a total model rate. Finally, we simulate the observed counts statistics by multiplying the total rates by the bin width in time to get total model counts for each time and energy bin. The counts are resampled randomly according to the Poisson distribution to obtain simulated observed counts. The total number of counts in each time bin determines the deadtime according to the GBM electronics model (Meegan et al. 2009). Together with the pulse model and background counts, these are saved in a FITS file that mimics

actual GBM data. Note that Basak & Rao (2012) have a similar procedure of pulse spectral evolution simulation, used for fitting burst lightcurves and spectra simultaneously. They used the E_{peak} evolution model of Liang & Kargatis (1996).

In real data, there is a certain level of background noise rate in each energy channel, usually changing (hopefully slowly) as a function of time. Modeling the background is important as it sets the scale of the signal versus noise for the entire simulation. Since our pulse model has an exponential rise and decay in time, it will be important to determine which spectra from our simulation have enough total counts to be usable for spectroscopy and which spectra may have to be added together (binned) with others in order to meet a preferred level of significance. In order to reduce the variance (especially important for low count spectral bins at higher energies), we start with a long background accumulation from actual burst data. Following our procedure for the BATSE and GBM spectroscopy catalogs (Kaneko et al. 2006; Goldstein et al. 2013; Gruber et al. 2014) we fit a low-order (≤ 4) polynomial to the temporal variations of the background and interpolate the fitted model during the burst interval. Usually, we select regions for background fitting both before and after the burst, to avoid the need to extrapolate the background model. Since the background is fit to a polynomial in time in each energy bin, the variance associated with each bin is governed by the Gaussian statistics of the background temporal model parameters (the fitted polynomial coefficients). This variance is recovered in our simulations by resampling the background counts from a normal distribution, given the background model error for that bin.

The resulting simulated pulse is remarkably simple, yet it reproduces a number of characteristics of observed single pulses. First of all, the light curve clearly mimics the observations, as expected, given that the Norris pulse model was designed for this purpose (e.g. Figure 3). We should mention that a pulse stacking analysis by Hakkila & Preece (2014) has shown that significant residuals exist on top of the Norris pulse shape that do not represent separate pulses; for example, there is a shoulder after the peak in Figure 3 at T+3 s as well as in the published GBM NaI light curve for GRB 130427A at roughly T+1.2 s. To keep the analysis

simple, we do not include this effect here. Upon performing spectral fitting of each time bin, the simulated power-law E_{peak} evolution from hard to soft ($E_{\text{hi}} = 1500$ keV and $E_{\text{lo}} = 100$ keV) is recovered from the simulation, as can be seen in Figure 4. In this simulation, the peak count rate was chosen to be extremely high, 40,000 count/s, even so, during the rise and decay portion of the pulse some low-count time bins had to be combined to achieve a minimum signal to noise threshold of 45. This threshold ensures that there are enough total counts in the binned spectra to do useful spectroscopy, as described in the BATSE and GBM Spectroscopy Catalogs.

We have checked the effect of the spectral parameter α by performing three identical simulations, varying only the α value in three steps between -0.66 and -1.2 , bracketing the most likely fitted value of -1 from the distributions reported in the various spectroscopy catalogs. For the three values simulated, there was no change in the mean value of E_{peak} for the resulting distributions to well within the uncertainty on the mean: 177 ± 2 keV (these and following simulations are based on $E_{\text{hi}} = 3000$ keV and $E_{\text{lo}} = 50$ keV). This is expected, as E_{peak} does not formally depend upon α (nor does it depend upon the Band parameter β , as long as $\beta < -2$). As discussed above, we do not present any simulations of Band functions, so the evolution of β is not considered here.

3.2. Spectral Lag and Pulse Width Evolution

This simulation of the temporal evolution of spectral parameters allows us to compare it with certain other properties of observed pulses, such as the spectral lag and pulse-width evolution as a function of energy, as characterized in the initial pulse of GRB 130427A (Preece et al. 2014). Because the simulations and the spectral fits share the same power law evolution model, the simulation reproduces the lag-width relation of the real data, when the lag is taken with respect to a fixed low energy channel. That is: the spectral lag increases as a function of increasing energy (Kocevski & Liang (2003); see Figure 5). In addition, the pulse width decreases with increasing energy (Richardson et al. (1996); see Figure 6). Except for the factor of ten increase in the timescales associated with the simulations, these

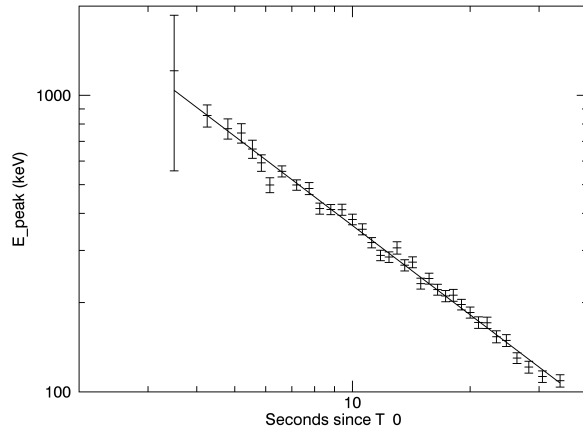


Fig. 4.— Fitted E_{peak} values from an example pulse simulation shows that the input -1 power law spectral evolution is recovered after signal-to-noise temporal binning and forward-folding with the detector response. In this case, the pulse parameters were 3 s rise time, 11 s decay time, scaled to 40,000 count/s at the peak. E_{peak} evolves from 1500 keV to 100 keV over the nominal duration of the pulse.

results are qualitatively consistent with the results presented in Figure 1 in Preece et al. (2014). One can visualize how this behavior arises by examining the joint temporal-spectral model as a contour plot. In Figure 7, we compare the fitted data from GRB130427A with the fitted data from our simulated pulse. Log energy is on the horizontal axis, while time is along the vertical. The energy of the peak in νF_ν (i.e.: E_{peak}) is traced over time by the dashed red line and can clearly be seen to exhibit a hard-to-soft trend, as indicated by movement toward the left in the plot. A vertical cut or band corresponds to a specific energy. The pulse peaks appear later in the lower energy bands, which is the source of the spectral lag. At the same time, the temporal power-law nature of E_{peak} ensures that an increasing number of spectra with similar E_{peak} values are found in a given accumulation time with respect to similar accumulations at the start of the pulse, where the spectra are varying more rapidly. This is the source of the increase in pulse temporal width with lower energy. It is interesting to speculate how this might be extended in the opposite direction in time with respect to the highest peak energies. The observed trend is

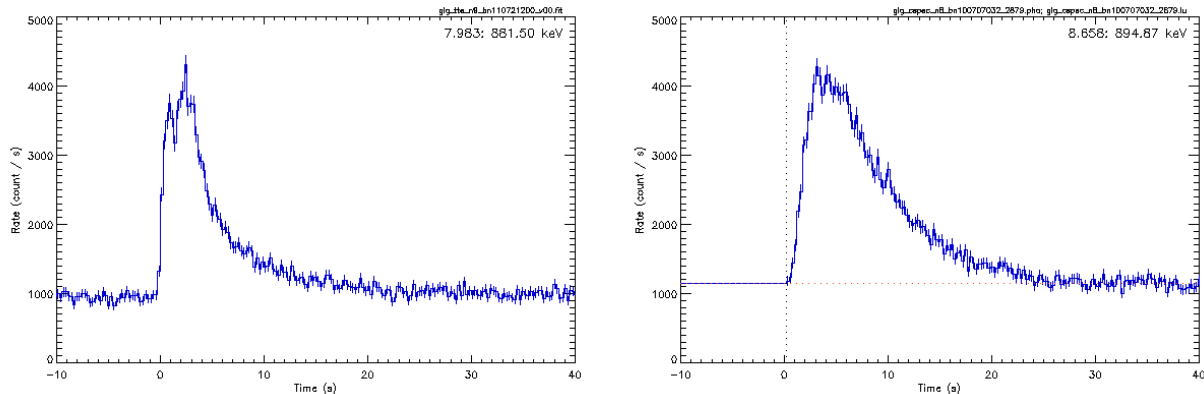


Fig. 3.— The GRB 110721A lightcurve from GBM NaI detector 9 at 256 ms time resolution shows some deviation from a simple pulse profile at the peak (left). Compare with a simulation derived from the Norris pulse model, with 3 s rise and 5 s decay time constants and 3000 count/s peak count rate scaling above background (right). The two figures are presented with the same x-axis limits; however no attempt was made to optimise the pulse parameters to make the simulated pulse profile match with the GBM data.

that the pulse width becomes increasingly narrow with higher energies at the same time that the pulse peak lag gets shorter, so that the temporal width approaches zero. The limiting result is that the highest energy photons are all confined to a very short time window very close to the GBM trigger time. Of course, real detectors are limited to counting photons, where the continuum model must break down. We note that there is a cluster of 3 Fermi LAT high-energy (> 100 MeV) photons in a 0.1 s window at or just before the GBM trigger time of GRB130427A, followed by a gap of 5 s.

The high intensity of this initial simulation allows us to examine the results with high temporal resolution. In particular, we can bin the fitted E_{peak} values according to number of occurrences in log energy, the result is shown in Figure 8. We have simulated a larger sample of spectra by using the time-resolved spectral fits from fifty simulations of bursts of varying brightness and different rise and decay parameters (Figure 9). The spectra were drawn from the set of simulations described below in Section 3.5, all binned to the same signal-to-noise criterion. Thus, the brightest simulated bursts contributed the most spectra at the highest temporal resolutions, while the dimmest bursts contributed few spectra, taken with relatively coarser binning. Clearly, as with the dimmer bursts from the actual observations,

the longer temporal accumulations can average over significant spectral evolution in a single spectrum.

The pulse histogram in Figure 8 clearly has the largest contribution from the portion in the lightcurve that is the most densely sampled; that is: from the region around the peak in the light curve, where E_{peak} doesn't change much. This is a sampling bias that can be seen even more dramatically in a histogram of the photon flux (Figure 10), which is sharply concentrated at the flux values near the peak of the lightcurves. Where E_{peak} is highest and lowest, the lightcurve is rapidly changing during the rise and decay portions, respectively, and thus the sampling of E_{peak} values is relatively sparser than at the peak of the lightcurve.

3.3. The Effect of Evolution in E_{hi}

So far, the simulations have only modeled one specific case of spectral evolution: they were all based upon the fixed values $E_{\text{hi}} = 1500$ keV and $E_{\text{lo}} = 100$ keV, resulting in the same value for the temporal decay index $i \approx -1$ (Eq. 6). Either one or both of these may naturally be considered to be drawn from a fairly large set of values, due to the spread in redshift and bulk Lorentz factors, as discussed in the Introduction (Eq. 3). We next investigate how these parameters influence the E_{peak}

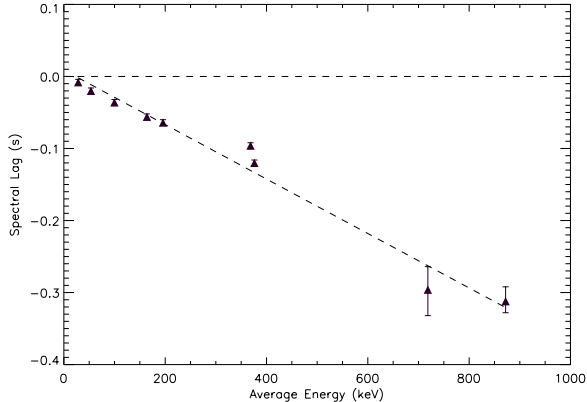


Fig. 5.— The spectral lag in seconds for the simulated pulse in Figure 4 is plotted against the average energy of 9 spectral data bins of roughly equal width in log energy. Some of the BGO detector bins overlap in energy with those of the NaI, which accounts for the odd spacing. The binning is the same as can be seen in Figure 6. The lowest energy bin serves as the reference against which the lag of the higher energy bins is calculated and thus has zero lag by definition.

distributions.

First, we generated pulse simulations by varying both E_{hi} and E_{lo} by the same factors of two: $(1/4, 1/2, 1, 2, 4)$. This has the effect of keeping the value of the temporal decay index i the same. The result could be predicted: the mean value for the resulting E_{peak} histograms for each pulse also change by the same factors of two. This behavior holds over the entire range of the inputs $E_{\text{hi}} = (750; 1,500; 3,000; 6,000; 12,000)$ keV (5 data points). This range was determined mainly by its effect on $E_{\text{lo}} = (12.5; 25; 50; 100; 200)$ keV: anything below 12.5 keV is not recoverable and anything above 200 keV is already too high to be very common, based upon the observed behavior that bursts with average or peak E_{peak} values greater than 1 MeV are rare. In any case, the linearity in the peak E_{peak} from this simulation suggests that one could build up any E_{peak} distribution whatsoever by weighting pulses with appropriate energy limit parameters. The most natural distribution prior for both E_{hi} and E_{lo} may be uniform, in which case, we should expect that the E_{peak} distributions be more flat-topped than they appear to be.

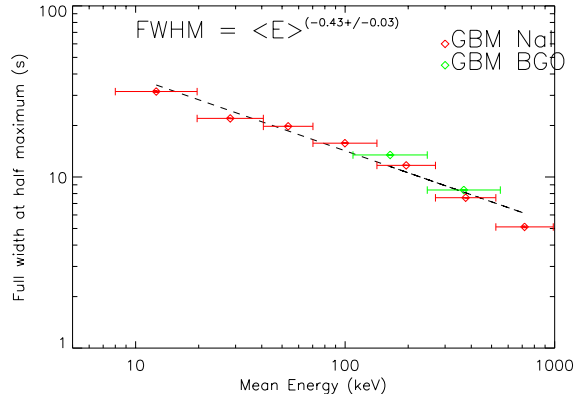


Fig. 6.— The pulse widths in different energy bands in seconds for the simulated pulse in Figure 4 is plotted against the average energy of each of the 9 spectral data bins of roughly equal width in log energy. The trend of wider pulse width for lower energy is fitted with a power law, as suggested by Norris et al. (2005).

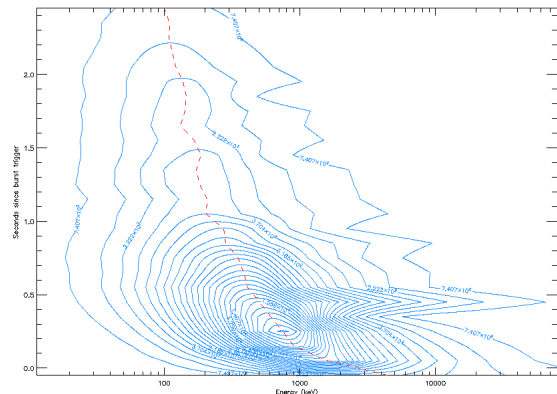


Fig. 7.— The spectral evolution of fitted E_{peak} values during the first 3 s of GRB130427A is presented as the ‘continental divide’ (dashed line) on top of a $\nu\mathcal{F}_\nu$ contour plot. Because E_{peak} represents the peak of each $\nu\mathcal{F}_\nu$ spectrum (arranged in time from bottom to top), the levels of increasing intensity form closed contours. The peak intensity clearly comes later than the highest E_{peak} , which is found at the start of the burst.

Next, we varied only E_{hi} by factors of two and kept E_{lo} constant. The corresponding change in the temporal decay index can be seen in Table 1. Here, we created 6 individual bright pulses with

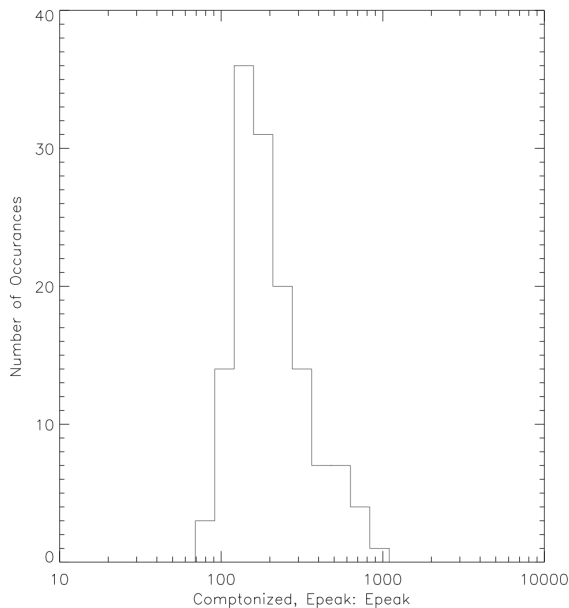


Fig. 8.— The distribution of fitted E_{peak} values for a simulation of a single, bright GRB pulse that has strong spectral evolution is shown as a histogram. Although the pulse is well sampled throughout its time history, the predominance of samples occurs at the peak of the pulse, heavily weighting the average spectrum with medium-energy E_{peak} spectra.

parameter values from $E_{\text{hi}} = 12,000$ to 375 keV. The mean E_{peak} values of the distributions do not change much: 270 to 93 keV, which is roughly a factor of 3 for a change by a factor of 32 in E_{hi} . Apparently, a large change in E_{hi} leads to only a modest shift in the E_{peak} distribution; the behavior of $\log(E_{\text{hi}})$ versus $\log(\langle E_{\text{peak}} \rangle)$ is definitely linear. As an aside, we could change the pulse parameters in each case to achieve a constant $i = -1$ decay index, but as these bright pulses are quite well sampled, it would make little to no difference in the results. A histogram of all the fitted E_{peak} values from these 6 simulated pulses is slightly skewed toward the low energy side, as seen in Figure 11. This arises because the distributions with lower E_{hi} are narrower, while they have roughly the same number of spectra. Despite this unbalanced weighting, the overall distribution still peaks at a median value, and is no more flat

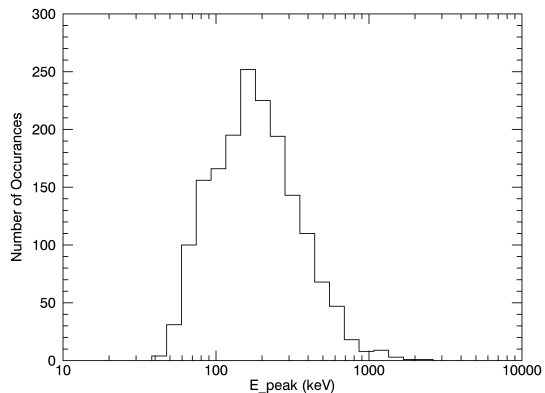


Fig. 9.— The distribution of fitted E_{peak} values is plotted as a histogram for fifty simulated single-pulse GRBs of ten different brightnesses and five different pulse asymmetries. Each simulated lightcurve has been binned to the same signal to noise ratio, resulting in different binning for each, while retaining similar statistics for the spectral fitting. The histogram represents the ensemble of all time-resolved spectra, similar to the BATSE or GBM Spectral Catalogs of Bright bursts, to be compared with Figure 1.

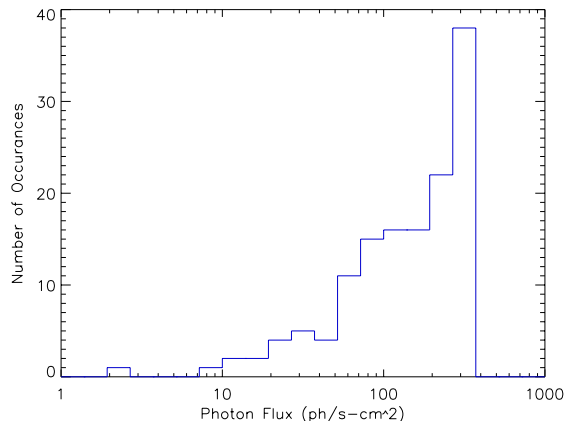


Fig. 10.— The distribution of photon flux values is displayed as a histogram for the bright single-pulse simulation shown in Figure 8. The single most populated bin corresponds with the peak in the lightcurve, which, by having the highest SNR, is the most frequently sampled portion of the lightcurve.

E_{hi} keV	$\langle E_{\text{peak}} \rangle$ keV	i Decay Index
12,000	272 ± 3	-1.45
6,000	218 ± 2	-1.16
3,000	177 ± 2	-1.08
1,500	143 ± 2	-0.9
750	115 ± 2	-0.71
375	93 ± 1	-0.53

Table 1: Results of simulations of bright, long pulses with different E_{hi} , but holding $E_{\text{lo}} = 50$ keV constant. The mean value of E_{peak} for each simulated time sequence is given by $\langle E_{\text{peak}} \rangle$. The temporal decay index is calculated from Eq. 6.

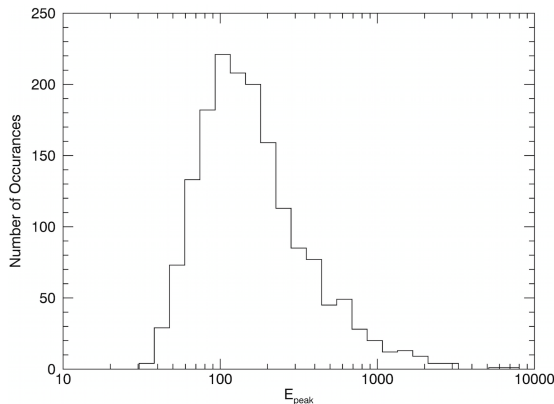


Fig. 11.— The distribution of fitted E_{peak} values is plotted as a histogram for six simulated single-pulse GRBs only differing in their values of E_{hi} .

topped than Catalog-derived distributions.

Which scenario may be preferred here depends upon what one expects as being more reasonable: is the temporal decay index of $i = -1$ a physical value, so we should scale both E_{hi} and E_{lo} by the same factor? We don't have a justification for this, but we have two examples of observed bursts with roughly this same temporal index (GRB110721A and GRB130427A): the durations scale in just such a manner to make this work. On the other hand, in the previous section, we put forth the hypothesis that pulses are initiated by an impulsive energization event that loses energy over time. In which case, only the initial E_{hi} value is important. Certainly, the maximum fitted E_{peak} values for the

two events are different by a factor of three or so. The value of E_{lo} would then be determined by the last point at which spectral fitting can be done on the decaying portion of the burst, not by any physical constraint. At the same time, a physical argument may support the concept of a conserved temporal decay index for this scenario as well: in order to maintain this index, the duration would certainly have to be coupled to the energy loss mechanism.

3.4. Spectral Characteristics of the Pulse-Averaged Spectrum

There are two things to note concerning the spectral fit to the average spectrum obtained by summing all the individual spectra in the simulated pulse. The first is that although the simulation was constructed with the cut-off power law function, the spectral evolution imposed throughout the pulse conspires to deform the average spectrum significantly. In fact, the pure cut-off power law function does not result in an acceptable fit, as evidenced by the significant runs of residuals to the spectral model, as seen in Figure 12 (*left*). As it happens, a fit to the same average spectrum using the Band function is much improved (CSTAT = 160, compared with CSTAT = 351, which is a considerable improvement for one degree of freedom; see Figure 12, *right*). Thus, at least for the HTS spectral evolution we have simulated, the sum of exponentially cut-off spectra can result in an average spectrum that is consistent with the Band function, which incorporates a high-energy power-law.

The other point is that the sampling bias shown in Figure 10 implies that values for E_{peak} derived from a fit to the average spectrum of a single-pulse burst should be very well correlated with that of the peak spectrum. The results for 11 single-pulse GRBs are shown in Table 2. The Pearson's rank correlation between the average and peak E_{peak} values is 0.77, which has a chance probability of 0.005. The 'peak' E_{peak} is given by $E_{\text{p,p}}$ and the average spectrum (or 'fluence') E_{peak} is $E_{\text{p,f}}$; both are in keV. In the last column in the Table, the difference between the peak and average spectra E_{peak} values is expressed in units of the r.m.s. errors of the two values. Not only are the peak values always greater than the average, but nearly every pair differ by less than three standard devi-

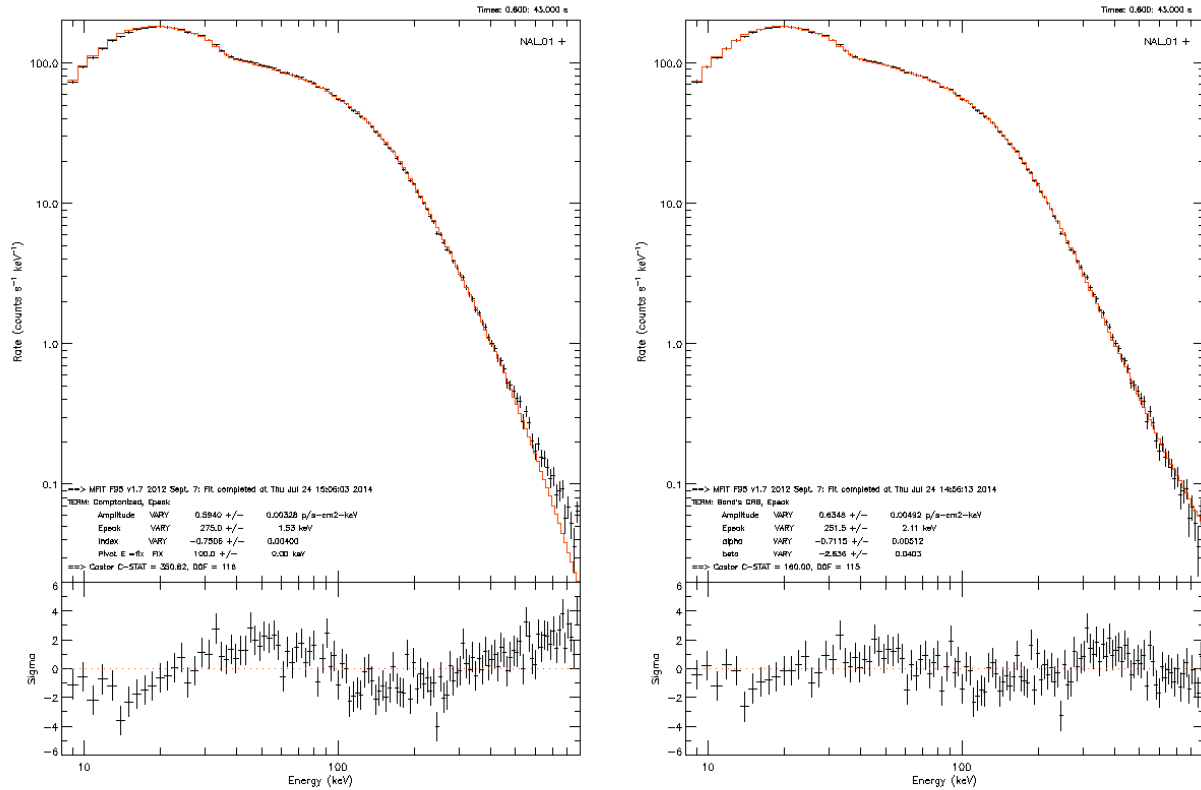


Fig. 12.— Time averaged spectral fits to the simulation of a very bright single-pulse GRB with strong spectral evolution (as described in Figure 4). The average spectrum is fitted with the input spectral function (cut-off model power law – COMP, *left*) as well as the Band function (*right*). The residuals plots at the bottom of the left-hand figure reveals strong discrepancies with the assumed COMP model that are largely absent in the Band function fit. The change in C-STAT between the two fits is 191 for one additional degree of freedom, suggesting that the sum of several COMP functions with strong evolution in E_{peak} and intensity do not preserve the COMP shape.

ations. For asymmetric pulses that peak early, the number of spectra after the peak in the lightcurve outnumber those before it, so a fluence-weighted spectrum will be dominated by lower E_{peak} spectra, compared with that of the peak spectrum itself, as discussed below. This accounts for the peak E_{peak} being greater than the fluence E_{peak} .

In GRB pulses, at least, it appears that there is a good correlation between the values of E_{peak} derived from fits to the peak and fluence spectra. Not all bursts are so strongly dominated by a single pulse in the light curve, yet we have made the case above that the spectral characteristics are

dominated by the sampling bias at the peak of the pulse. If bursts are typically made up of any number of discrete and overlapping pulses, the peaks of these pulses should still dominate their fluence spectra. We have tested this with fits to 1188 BATSE GRBs from the complete spectral catalog (Goldstein et al. 2013), as shown in Figure 13. The peak flux and fluence values are clearly correlated, with the best fit power law trend shown in red, along with the error bounds of the fit. The fitted power law function is $E_{\text{p,p}} = 1.41 \times E_{\text{p,f}}^{0.96}$, which also indicates the trend where the peak E_{peak} is larger than the fluence E_{peak} . The Pearson correlation coefficient (linearity in log-space)

GRB	$E_{p,p}$	$E_{p,f}$	Sigma Dev.
081110601	192 ± 49	46 ± 12	2.8
081224887	934 ± 217	361 ± 30	2.6
090719063	361 ± 39	207 ± 8	3.8
090809978	227 ± 40	158 ± 10	1.6
100612726	143 ± 10	111 ± 4	2.7
100707032	597 ± 63	239 ± 10	5.6
110407998	779 ± 309	543 ± 106	0.6
110721200	1506 ± 756	237 ± 32	1.7
110817191	345 ± 40	207 ± 16	3.2
110920546	902 ± 279	215 ± 5	2.5
130427324	812 ± 19	784 ± 9	1.3

Table 2: Comparison between Peak and Fluence E_{peak} . Column 1 lists the burst name in the GBM convention (yymmddfff; see Paciesas et al. (2012)). Columns 2 and 3 show the fitted E_{peak} value in keV for the peak flux and the fluence spectra, respectively. The last column shows the difference between the two E_{peak} values in units of the root mean square of the two error values.

is 0.895 ± 0.003 , and the Spearman rank coefficient (monotonicity) is 0.892 ± 0.003 . The uncertainty assumes the Epeak errors are (log-)normally distributed. One possible consequence of this correlation is the correspondence between Amati-like relations that use the fluence-based E_{peak} (Amati et al. 2002) and the Yonetoku-like relations that use the peak E_{peak} (Yonetoku et al. 2004; Ghirlanda, Ghisellini & Lazzati 2004): they are basically the same value. In our picture of strong spectral evolution within pulses, the E_{peak} value for the fluence spectrum is dominated by the heavy weighting by the spectra close to peak of the pulse, as they contain the majority fraction of the counts in the fluence.

3.5. The Role of Pulse Asymmetry

We have shown above that the peak spectra dominate the fluence-derived E_{peak} value for a pulse with strong spectral evolution. Clearly, there should be an effect on this derived value that depends upon where in the pulse history the peak lies: early or late. If the pulse rises quickly, the peak spectra will sample the earlier values of the E_{peak} evolution trend and thus should be higher on average. The opposite case holds for pulses that peak later relative to the overall pulse dura-

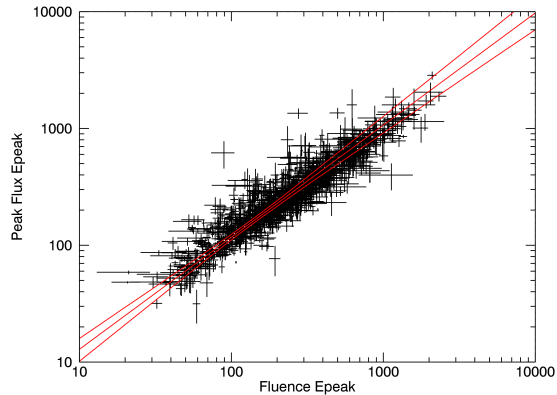


Fig. 13.— The values of fitted E_{peak} for time-averaged (‘fluence’) spectra are plotted against the fitted E_{peak} values from the peak flux spectrum for the same burst. The 1188 GRBs are from the BATSE Spectroscopy Catalog (Goldstein et al. 2013), where the best fits were either COMP or BAND and the E_{peak} values were constrained.

tion. Hakkila & Preece (2011) have shown that the majority of bright pulses in their catalog are asymmetric and that the asymmetry is generally correlated with spectral hardness (Hakkila et al. 2015).

Following the sources cited above, we define the pulse asymmetry at the level of e^{-3} of the peak intensity as:

$$\kappa = \frac{1}{\sqrt{1 + 4\sqrt{\tau_1/\tau_2}/3}}. \quad (8)$$

This quantity ranges from $\kappa = 1$, for an early-peaking asymmetric pulse, to $\kappa = 0$, for a symmetric pulse (the peak divides the duration in two). Note that the two pulse shape parameters of the Norris pulse model (τ_1 & τ_2) do not directly map into the rise time or decay time of the pulse. Formally, the rise and decay times may be determined from the shape constants by the expressions

$$\tau_{\text{rise}} = \frac{n\tau_2}{2} \left[\sqrt{1 + 4\sqrt{\tau_1/\tau_2}/n} - 1 \right],$$

and

$$\tau_{\text{decay}} = \frac{n\tau_2}{2} \left[\sqrt{1 + 4\sqrt{\tau_1/\tau_2}/n} + 1 \right], \quad (9)$$

where, as above, we take $n = 3$. Indeed, the shape

parameters from the last line in the Table, $\tau_1 = 150$ s and $\tau_2 = 1$ s, produce an approximately symmetric pulse, while the values from the first line, $\tau_1 = 6$ s and $\tau_2 = 5$ s, result in a very fast rise, slower decay pulse with high early-peaking asymmetry. Pulses with late-peaking asymmetry can not be modeled (because of the constraint $\kappa \geq 0$). Late-peaking pulses are rare in the published literature of GRB pulse modeling.

We constructed five separate sets of synthetic GRB spectral histories, each with different values for τ_1 and τ_2 , resulting in five different values for κ . In each set, we created 10 bursts with different peak count rates: 10,000, 9,000, 8,000, 7,000, 6,000, 5,000, 4,000, 3,000, 2,000 and 500 count/s. Averaging the spectral fits over each set should smooth out difficulties that arise with the pulse model: for instance, the pulse width (t_{dur}) is defined with respect to the 3 e -folding decrease on either side of the pulse peak. Depending on the overall intensity of the pulse, this value may differ significantly from the duration, either derived formally (e.g.: as T_{90} , the duration of 90% of the flux (Koshut et al. 1996)) or determined by eye. When the exponential rise begins and the tail ends depends upon the signal to noise of each spectrum in the sequence.

The results of this analysis, as presented in Table 3, show that there is a trend toward higher E_{peak} values for higher values of asymmetry (κ in the Table). This trend is seen both for the highest count-rate simulation ('10k E_{peak} ' column), as well as the for the average over the ensemble of weak to bright pulses. The relation between the pulse parameters, especially the position (in time) of the peak, and the derived duration, are complicated by the definition of pulse duration in terms of number of e -foldings of the rise and decay exponentials. As seen in the last row of the table, the peak time seems to be equal to the duration; in such cases, the start time of the duration is delayed. Accordingly, we include the rise and decay times (τ_{rise} and τ_{decay}), as calculated by Equation 9, in columns 6 and 7. Still, the general trend may be described as correlation between asymmetry and E_{peak} : the later the pulse peaks, the lower the fluence-averaged E_{peak} value that will be obtained for the same power-law spectral evolution in a pulse.

4. More Complicated Lightcurves

Most GRB lightcurves are not as simple as our single-pulse model. Some consist of well-separated (or, at least: clearly overlapping) single pulses, such that the pulses can be individually fitted (see, for example, the pulse catalogs in Ford et al. (1995); Hakkila & Preece (2011); Lu et al. (2010)). A main result of these efforts was that individual pulses within bursts could be categorized into two broad classes based upon their spectral evolution: hard-to-soft (HTS) and hardness-intensity tracking (HIT), as discussed above. So far, we have focused on HTS pulses. As long as separable pulses can be identified within a complex light curve, the results we have identified so far should hold for more complex bursts, as long as each pulse belongs in the HTS category. The existence of the HIT category raises several issues, then: can we determine the relationship between the peak flux and fluence values for E_{peak} ; and, can we account for HIT evolution within the context of HST evolution pulses?

As Figure 10 demonstrates, burst lightcurves are the most heavily sampled at the peak. The result is that the time-averaged ('fluence') spectrum is heavily weighted by those spectra, resulting in an average fitted E_{peak} value that represents them. This should be true of pulses with HIT spectral evolution as well: the softer spectra at the rise and tail of the pulse are underrepresented in the average, just as they are in HTS pulses. In this case, instead of very hard spectra being under-sampled during the rising portion of the pulse, the rising portion of the HIT spectral evolution mirrors the decay in time, so no spectra are harder than those at the peak of the pulse. Thus, regardless of whether the pulse is HTS or HIT, the fluence E_{peak} should correlate well with that of the peak flux spectrum within a burst. HIT pulses should not destroy the correlation found in Figure 13.

More interesting is the question of generating HIT pulses within the HTS pulse paradigm. Where two HTS pulses overlap, the combined spectra are likely to be dominated by the more intense of the two, especially when signal-to-noise binning is taken into account. Thus, we should expect that the least intense, very hard spectra at the rise portion of a later pulse to be completely

τ_1 (s)	τ_2 (s)	κ	τ_{peak} (s)	τ_{dur} (s)	τ_{rise} (s)	τ_{decay} (s)	10k E_{peak} (keV)	Ave. E_{peak} (keV)
6	5	0.64	5.5	23.5	4.3	19.3	297 ± 9	303 ± 29
3	5	0.70	3.9	21.4	3.2	18.2	241 ± 5	262 ± 54
6	3	0.59	4.2	15.3	3.1	12.1	200 ± 5	224 ± 43
20	3	0.47	7.7	19.0	5.0	14.0	153 ± 3	155 ± 9
150	1	0.24	12.2	12.5	4.7	7.7	79.5 ± 1	83 ± 6

Table 3: Fluence E_{peak} and Pulse Asymmetry. A series of simulations were performed to demonstrate the effect of pulse asymmetry for a standard spectral evolution model during each pulse. Columns 1 and 2 contain the pulse rise and decay parameters (τ_1 & τ_2); ten simulations were created for each of these pulse shape values, where the pulse peaks were scaled as described in the text. The derived asymmetry (κ), the peak time (τ_{peak}), duration (τ_{dur}) and the rise and decay times of the pulse (τ_{rise} and τ_{decay}) follow in columns 3 – 7. Column 8 gives the E_{peak} value for the single 10,000 count/s run (the brightest in each set of ten), while the last column gives the average of the fitted E_{peak} values for the ten runs in each set.

dominated by softer spectra on the decay tail of the preceding pulse. This will continue until the spectra from the following pulse start to dominate the spectral fits, which should occur near the peak intensity of the later pulse, if it rises sufficiently rapidly. In order to determine what happens in the transition region where the intensities are roughly equal but the individual pulses contribute E_{peak} values that are considerably different, we turn back to simulations. Figure 14 shows the result of several overlapping pulses, each with the same rise and decay times (3.0 and 11.0 s), the same intensities (10000 count/s), the same E_{peak} evolution parameters (1500. to 100. keV), but increasing start times: 0, 1, 2, 4, 8, 16, and 32 s. There is no physical motivation for this time series. The first four pulses blend together into one relatively intense pulse, which has not lost the overall HTS spectral evolution of its constituents. The last two pulses however, demonstrate classic HIT behavior. The possibility that isolated pulses may actually be comprised of a train of subpulses was raised by Hakkila & Preece (2014), who discovered a conserved pattern of residuals after subtracting the Norris pulse model fit from observed pulses and stacking the residuals. There is an indication for a hardening in each of the sub-pulses, as observed in Figure 14. A full treatment of this question is somewhat outside of the main scope of the present work; we hope to address it more completely in a later paper.

5. Discussion

Out of the many E_{peak} values that can be found in any given burst, the question of which E_{peak} can represent the burst to the extent that it can be an accurate cosmological indicator has at least two robust answers: both the time-averaged and peak flux-derived values, due to their correlation. The details of spectral evolution, pulse asymmetry and pulse shape apparently conspire with signal-to-noise temporal binning to pick out a medium energy value from a span that can cover at least a decade.

We have constructed a simulation that reproduces the time history and spectral evolution found in detail for at least two bright pulses in observed GRBs, as well as qualitatively in several other observed single-pulse bursts. Using this pulse simulation, we are also able to determine why the fitted values of E_{peak} are so highly correlated between the time averaged and peak flux spectra in GRBs: a signal-to-noise temporal binning of spectra within a burst profile strongly biases the number of spectra at the peak of pulses. This has the effect of creating a large number of spectra during a relatively narrow time window, where E_{peak} doesn't change much and is mid-way through its evolution from hard to soft. The peak flux spectrum picks out an E_{peak} value that is far from the extremes of its evolution, while the fluence spectrum has the spectral characteristics near the peak of the pulse as the overwhelming contributor to the average. A more subtle consequence of

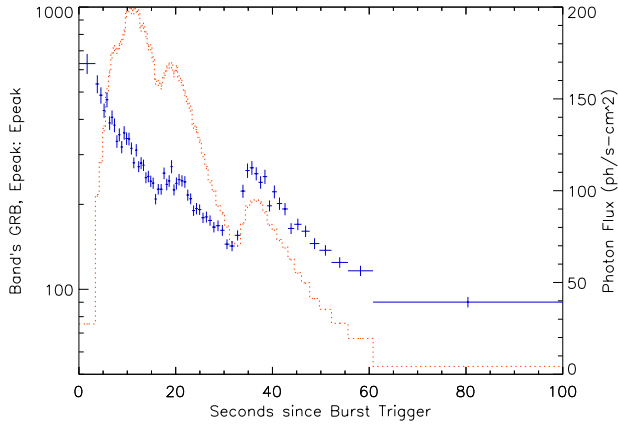


Fig. 14.— The spectral evolution of one simulation of a complex lightcurve shows both hard-to-soft and hardness-intensity-tracking behavior in E_{peak} . The left and right axes correspond to E_{peak} (in keV) and photon flux, respectively. The parameters of the simulation are detailed in the text, but can be described as seven identical pulses with an overlap in time that is spaced in a geometric progression series with a common ratio of 2.

the predominance of peak spectra sampling comes in the interpretation of the E_{peak} distributions as presented in time-resolved spectral catalogs of GRBs (e.g. Kaneko et al. (2006)). GRB spectra clearly can have very high and very low E_{peak} values and we have shown that the fitting process does not add very much dispersion to the distribution. So, how does the observed distribution with a FWHM of approximately a decade in energy arise? Our pulse simulations have shown that: either the limiting energy parameter priors are such that there are no constraints, in which case some unknown mechanism is at work to create the shape of observed distribution. Or else pulses act like our impulsive model, defined by the highest energy at the pulse leading edge, which does have the effect of selecting out the median energies for peak flux and fluence spectra, resulting in the observed narrow distributions.

It is reasonable to ask whether the use of a temporal binning scheme other than signal-to-noise might have an impact on our results. The Bayesian Block (BB) histogram representation of time series data is a method that can optimally capture the statistically important features of the

data (Scargle et al. 2013). For example, a Poisson-dominated time series that is constant within a predefined measure of probability would be represented by a single bin in the Bayesian Block scheme. This has the advantage of capturing quiescent periods between pulses in a single time bin that can be omitted from further analysis. For the same time series, a signal-to-noise binning might extend an incomplete time bin at the trailing edge of one pulse through a quiescent period into the rising portion of the next pulse before sufficient counts above background have been accumulated to fill out the bin. Thus, one scheme creates a good representation of the peaks and valleys of a complex light curve (BB), while the other accumulates bins of equal statistical weights (SNR). For time-resolved spectroscopy, the SNR representation gives binning of equal statistics, so that the spectra can be compared within single bursts and between different bursts. The BB binning would tend to assign the peak into a single bin, which is approximately constant, while breaking up a fast rising (or falling) portion into many bins, some of which may be sub-optimal for spectral fitting. Of course, the BB binning criteria can be adjusted until every bin has at least the minimum SNR for spectral fitting, perhaps at the expense of allowing some bins to have much higher weighting. So far, no comprehensive time-resolved spectroscopy catalog has used this method, although it was a feature of the analysis of a selection of single-pulse bursts by Burgess et al. (2014). This approach allowed for excellent determination of the spectral parameters of their model.

The HTS spectral evolution we have considered here as an archetype for the GRB pulse profile has quite profound physical implications. In particular, the higher energies are concentrated (by the dual action of narrowing pulse widths and decreasing spectral lags) into shorter intervals of time occurring earlier in the pulse. This is borne out in the case of extremely high energies in the first pulse of GRB 130427A, where three LAT photons (> 100 MeV) are observed within 0.1 s either way around the GBM trigger time, followed by a gap of roughly 5 s., during which only one other photon above 100 MeV is observed (Preece et al. 2014). There is a wider distribution of LAT LLE photons (30 – 100 MeV), with a FWHM of roughly 0.4 s surrounding the higher energy LAT photons (Ack-

ermann et al. 2014). Clearly, bursts are *capable* of producing the highest energy photons impulsively. That being the case, questions arise concerning the nature of the pulse as seen in lower energies, as covered by BATSE or GRB NaI detectors. Perhaps the entire evolution of the pulse driven by an impulsive event that somehow rapidly fills up a reservoir of energy that is released over time, as proposed by Liang & Kargatis (1996), Kocevski & Liang (2003) and Basak & Rao (2012). In accounting for the spectral lag evolution in GRB pulses as a function of the running integrated photon fluence,

$$E_{\text{peak}} = E_0 e^{-\Phi(t)/\Phi_0}, \quad (10)$$

these authors do not address the *pulse* flux evolution that drives the running fluence $\Phi(t)$. Left unanswered is why there should be a rising edge to the pulse, rather than, say, an abrupt turn-on or even a simple decaying exponential shape, neither of which is commonly observed in GRBs, if at all. In our impulsive model, the pulse rise occurs as the bulk of the cooling photons enter into the detector passband from above, until the peak, when all the higher energy photons have been degraded. The rest of the lightcurve is then seen as a cooling curve, with some photons moving into the X-ray band and dropping out of view. A impulsively illuminated, thin-shell, relativistic flow exhibits rise, decay and asymmetric pulse behavior simply due to curvature effects, as described by Dermer (2004). In addition, a kinematic treatment predicts that the instantaneous $\nu\mathcal{F}_\nu$ flux should behave as E_{peak}^3 during the pulse decay phase. This seems to be at odds with some of the observed pulse spectral evolution (Borgonovo & Ryde 2001). Preece et al. (2014) have addressed this by invoking magnetic reconnection or mini-jets as the impulsive event, followed by magnetic flux freezing in the expanding fluid element.

The less intense a pulse is (as in dimmer GRBs), the more bins around the pulse peak must be included to maintain a constant SNR for spectroscopy; however, given the nearly constant spectral evolution at the peak, the larger number of bins included in the fit does not affect the mean E_{peak} . With HTS spectral evolution, we expect the peak E_{peak} to be robust with respect to intensity for even the broadest binning required for the dimmest bursts. We have done an analysis of the peak flux spectra from the 50 simulated

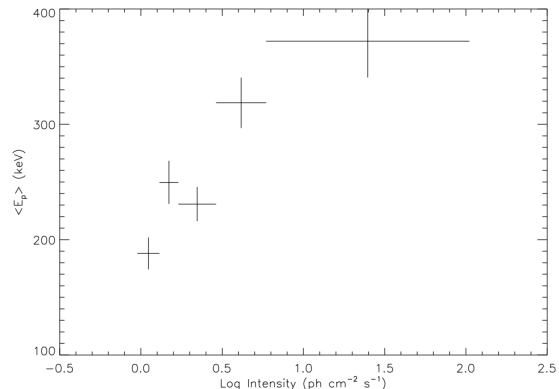


Fig. 15.— The average peak $\nu\mathcal{F}_\nu$ energies as a function of intensity for five groups of peak flux spectra from 1421 BATSE GRBs. The horizontal error bars indicate the intensity bin widths, while the vertical error bars represent the the 1σ errors in the mean, where the E_{peak} distributions were assumed to be approximately Gaussian in log energy.

pulses described in Table 3 (which divides into ten peak flux groups) that shows no change in average E_{peak} values from dimmest to brightest: the slope in average E_{peak} as a function of peak flux is only 0.1σ different from 0, with 99.99% confidence. Thus, in the model where bursts are composed entirely from separable pulses (even if they can not be separated formally), observed correlations between peak flux E_{peak} and peak intensity are almost certainly intrinsic in nature. With 399 bursts from an early version of the BATSE Spectroscopy Catalog, Mallozzi et al. (1995) demonstrated that there is a significant correlation between the peak intensity and mean E_{peak} for five intensity groups. We have repeated this analysis using the complete catalog with 1421 bursts (Goldstein et al. (2013), or 3.5 times as many bursts as in the Mallozzi data set), as shown in Figure 15. The strong shift in mean E_{peak} as a function of intensity that is replicated here must be intrinsic, and follows the trend expected from standard cosmology, as was pointed out by Mallozzi et al. (1995).

6. Conclusions

Given that pulse peaks of GRBs pick out a representative value of E_{peak} , the answer to the ques-

tion posed in the Abstract, “Which E_{peak} ?” is: “The peak flux E_{peak} ”. We have shown that a simple pulse model with HTS spectral evolution can account for several observables:

- the narrow E_{peak} distributions found in several spectral catalogs;
- the fluence and peak flux E_{peak} correlation;
- the role of pulse asymmetry on the average E_{peak} ;
- the constraint of the temporal decay index to observed values for widely different values of E_{hi} ;
- the impulsive nature of pulse energization; and
- the frequent observation that the first spectrum in a burst is the hardest.

In addition, these results are robust, even to the point that we need only assume that a pulse has *some* type of spectral evolution, either HTS or HIT. The latter may be gotten by layering HTS pulses on top of each other. Finally, bursts with multiple pulses can be thought of a collection of average spectra for the individual pulses, each of which is represented by the average E_{peak} at the peak. We don’t yet have a theory for the spectral evolution of *pulses*; however, to the extent that bursts are generally HTS, the peak E_{peak} of this distribution, as observed in the spectral window of the detector, should dominate the burst itself.

Acknowledgements

We are grateful for the comments on the first draft of this manuscript made by the anonymous referee. We had overlooked a crucial aspect of the analysis and the paper is much improved as a result.

REFERENCES

Ackermann, M., Ajello, M., Asano, K., et al. 2014, *Science* 343, 42

Amati, L., Frontera, F., Tavani, M., et al. 2002, *A&A*, 390, 81

Axelsson, M., Baldini, L., Barbiellini, G., et al. 2012, *ApJL*, 757, L31

Band, D. L. & Preece, R. D. 2005, *ApJ*, 627, 319

Band, D., Matteson, J., Ford, L., et al. 1993, *ApJ*, 413, 281

Baring, M. G. 2006, *ApJ*, 650, 1004

Baring, M. G., & Harding, A. K. 1997, *ApJ*, 491, 663

Basak, Rupal & Rao, A. R., 2012, *ApJ* 749, 132

Borgonovo, L., & Ryde, F. 2001, *ApJ*, 548, 770

Burgess, J. M., Preece, R. D., Connaughton, V., et al. 2014, *ApJ*, 784, 17

Cucchiara, A., Levan, A. J., Fox, D. B., et al. 2011, *ApJ*, 736, 7

Dermer, C. D. 2004, *ApJ*, 614, 284

Ford, L. A., Band, D. L., Matteson, J. L., et al. 1995, *ApJ*, 439, 307

Galama, T. J., Vreeswijk, P. M., van Paradijs, J., et al. 1998, *Nature*, 395, 670

Ghirlanda, G., Ghisellini, G., & Lazzati, D. 2004, *ApJ*, 616, 331

Goldstein, A., Preece, R. D., Malozzi, R. S., et al. 2013, *ApJS*, 208, 21

Gruber, D., Goldstein, A., Weller von Ahlefeld, V., et al. 2014, *ApJS*, 211, 12

Hakkila, J., & Cumbee, R. S. 2009, *American Institute of Physics Conference Series*, 1133, 379

Hakkila, J., Lien, A., Sakamoto, T., et al. 2015, *ApJ*, 815, 134

Hakkila, Jon & Preece, Robert D., 2011, *ApJ* 740, 104

Hakkila, Jon & Preece, Robert D., 2014, *ApJ* 783, 88

Harris, M.J. & Share, G.H., 1998, *ApJ*, 494, 724

Kaneko, Y., Preece, R. D., Paciesas, W. S., Meegan, C. A., & Band, D. L. 2006, *ApJS*, 166, 298

Kocevski, Dan & Liang, Edison, 2003, *ApJ* 594, 385

- Koshut, T. M., Paciasas, W. S., Kouveliotou, C., et al. 1996, *ApJ*, 463, 570
- Liang, Edison & Kargatis, Vincent, 1996, *Nature* 381, 49
- Lu, R.-J., Hou, S.-J., & Liang, En-Wei, 2010, *ApJ* 720, 1146
- Mallozzi, R. S., Paciasas, W. S., Pendleton, G. N., et al. 1995, *ApJ*, 454, 597
- Mazets, E.P. & Golenetskii, S.V., 1981, *ApSS*, 75, 47
- Meegan, C., Lichti, G., Bhat, P. N., et al. 2009, *ApJ*, 702, 791
- Metzger, A. E., Parker, R. H., Gilman, D., Peterson, L. E., & Trombka, J. I. 1974, *ApJ*, 194, L19
- Nakar, E., & Piran, T. 2005, *MNRAS*, 360, L73
- Nava, L., Salvaterra, R., Ghirlanda, G., et al. 2012, *MNRAS*, 421, 1256
- Norris, J. P., Nemiroff, R. J., Bonnell, J. T., et al. 1996, *ApJ*, 459, 393
- Norris, J. P., Bonnell, J. T., Kazanas, D., et al. 2005, *ApJ*, 627, 324
- Paciasas, W. S., Meegan, C. A., von Kienlin, A., et al. 2012, *ApJS*, 199, 18
- Piran, T., Sari, R. & Mochkovitch, D., 2012, in *Gamma Ray Bursts*, ed. Kouveliotou, Wijers & Woosley (Cambridge, UK: Cambridge Univ. Press), 121
- Preece, R., Burgess, J. M., von Kienlin, A., et al. 2014, *Science*, 343, 51
- Rees, M. J., & Mészáros, P. 1994, *ApJ*, 430, L93
- Richardson, G., Koshut, T., Paciasas, W., & Kouveliotou, C. 1996, *American Institute of Physics Conference Series*, 384, 87
- Scargle, J. D., Norris, J. P., Jackson, B., & Chiang, J. 2013, *ApJ*, 764, 167
- Schaefer, Bradley E. & Collazzi, Andrew C., 2007, *ApJ* 656, L53
- Yonetoku, D., Murakami, T., Nakamura, T., et al. 2004, *ApJ*, 609, 935

This 2-column preprint was prepared with the AAS L^AT_EX macros v5.2.